Nationaal Lucht- en Ruimtevaartlaboratorium

National Aerospace Laboratory NLR

Executive summary

Prediction of wind turbine noise and validation against experiment

directivity

swish
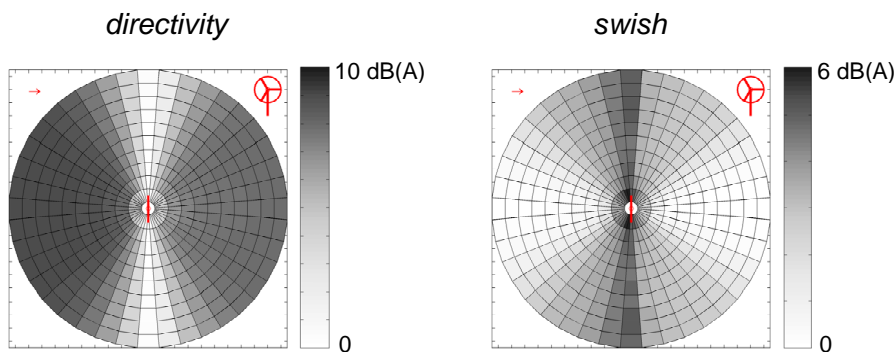
Problem area
The availability of fast and accurate wind turbine noise prediction methods is important for the design of quiet wind turbines and for the planning of wind farms.

Description of work
A semi-empirical prediction method for trailing edge noise is applied to calculate the noise from two modern large wind turbines. The prediction code only needs the blade geometry and the turbine operating conditions as input. The availability of detailed acoustic array and directivity measurements on the same turbines enables a thorough validation of the simulations.

Results and conclusions
The prediction code is successfully validated against the experimental results, not only with regard to sound levels, spectra, and directivity, but also with regard to the noise source distribution in the rotor plane and the temporal variation in sound level (swish). The validated prediction method is then applied to calculate wind turbine noise footprints, which show that large swish amplitudes can occur even at large distance.

Applicability
This study provides a firm validation of the prediction method, which therefore is a valuable tool for the design of quiet wind turbines and for the planning of wind farms.

Prediction of wind turbine noise and validation against experiment

NLR-TP-2009-402

Prediction of wind turbine noise and validation against experiment

S. Oerlemans and J.G. Schepers[1]

[1] ECN

Customer	NLR
Contract number	----
Owner	NLR
Division NLR	Aerospace Vehicles
Distribution	Unlimited
Classification of title	Unclassified
	October 2009

Approved by:

Author	Reviewer	Managing department
SO 19/10/09	*PS* 19-10-09	2/10

Contents

This page is intentionally left blank.

Prediction of wind turbine noise and validation against experiment

S. Oerlemans*

National Aerospace Laboratory NLR, P.O. Box 153, 8300 AD Emmeloord, Netherlands

J. G. Schepers

Energy Research Centre of the Netherlands ECN, P.O. Box 1, 1755 ZG Petten

ABSTRACT

A semi-empirical prediction method for trailing edge noise is applied to calculate the noise from two modern large wind turbines. The prediction code only needs the blade geometry and the turbine operating conditions as input. Using detailed acoustic array and directivity measurements, a thorough validation of the predictions is carried out. The predicted noise source distribution in the rotor plane (as a function of frequency and observer position) shows the same characteristics as in the experiments: due to trailing edge noise directivity and convective amplification, practically all noise (emitted to the ground) is produced during the downward movement of the blades, causing an amplitude modulation of broadband aerodynamic blade noise at the blade passing frequency ('swish'). Good agreement is also found between the measured and predicted spectra, in terms of levels and spectral shape. For both turbines, the deviation between predicted and measured overall sound levels (as a function of rotor power) is less than 1-2 dB, which is smaller than the scatter in the experimental data. Using a smoothed analytical trailing edge noise directivity function, the turbine noise directivity is predicted within 1-2 dB, and the swish amplitude in different directions within 1 dB. This semi-empirical directivity function shows similar characteristics as the theoretical directivity function for a flat plate, except for regions close to the plane of the blade. The validated prediction code is then applied to calculate noise footprints of the wind turbine as a function of rotor azimuth. These footprints show that for cross-wind directions the *average* level is lower than in the up- and downwind directions, but the *variation* in level is larger. Even at large distance, swish amplitudes up to 5 dB can be expected for cross-wind directions.

1. INTRODUCTION

Wind is a clean and practically inexhaustible source of energy. However, the noise of wind turbines is a major hindrance for the widespread use of wind energy. A recent survey on the perception of wind farms in the Netherlands [1] showed that sound was

*Corresponding author, Tel: +31-527-248642; Fax: +31-527-248210; E-mail: stefan@nlr.nl

the most annoying aspect of wind turbines. The swishing character (amplitude modulation) of the noise was mentioned as an important factor explaining the relatively high annoyance, as compared to other sound sources of equal level (air or road traffic). For the design of quiet wind turbines, and for the planning of wind farms, the availability of fast and accurate noise prediction methods is essential. In order to have a wide range of application, prediction codes should capture the physical source mechanisms as much as possible.

For a modern large wind turbine, aerodynamic noise from the blades is generally considered to be the dominant noise source, provided that mechanical noise is adequately treated [2]. The sources of aerodynamic noise can be divided into airfoil self-noise and inflow-turbulence noise. Airfoil self-noise is the noise produced by the blade in an undisturbed inflow, and is caused by the interaction between the boundary layer and the trailing edge of the blade. Self-noise can be tonal or broadband in character, and may be caused by several mechanisms, such as turbulent boundary layer trailing edge interaction noise (subsequently denoted as trailing edge noise), laminar boundary layer vortex shedding noise, trailing edge bluntness noise, or blade tip noise. Inflow-turbulence noise is caused by the interaction of upstream atmospheric turbulence with the leading edge of the blade, and depends on the atmospheric conditions. It is an open issue to what extent inflow-turbulence noise contributes to the overall sound level of a wind turbine [3].

Due to the large number of applications (for example wind turbines, airplanes, helicopters, fans), the characteristics of airfoil noise have been investigated extensively in both experimental and theoretical studies [4–22]. Inflow-turbulence and self-noise mechanisms were considered and the dependence on parameters such as flow speed, angle-of-attack, radiation direction, and airfoil shape was characterized. These investigations formed the basis of several semi-empirical wind turbine noise prediction methods, which were assessed by comparison with field measurements [23–32]. In most cases the prediction methods included trailing edge noise and inflow turbulence noise. However, since the field results only provided the total sound level of the turbine, and sometimes part of the turbine noise was attributed to other sources, such as tip noise or mechanical noise, only an indirect validation of the prediction codes was possible. Furthermore, in none of these studies the noise directivity or swish amplitude was predicted and compared with experimental results.

A number of studies have addressed the swish phenomenon experimentally [33–39]. Swish is here defined as the amplitude modulation of broadband aerodynamic blade noise at the blade passing frequency (typically around 1 Hz). Refs. [36–38] reported detailed source localization measurements on two modern large wind turbines, using a large microphone array positioned about one rotor diameter upwind of the turbine. The array results showed that practically all noise perceived on the ground was produced by the outer part of the blades (but not the very tip), during their downward movement. This strongly asymmetric source pattern, which caused the swishing noise during the passage of the blades, was explained by trailing edge noise directivity and convective amplification. Moreover, in [36] it was shown that the source pattern could *only* be explained by trailing edge noise directivity (and not by inflow-turbulence noise or low-frequency dipole noise). Several investigations [33–35,39] reported periods of

increased amplitude modulation (also referred to as 'thumping'), which could be observed at large distance. Although various possible causes for this increased amplitude modulation have been suggested, including blade noise directivity, blade-tower interaction, variation of wind speed over the rotor, and interaction between the noise from two or more turbines, the mechanism is still not clear.

The present study describes the application of a semi-empirical prediction method for trailing edge noise to calculate the noise from two modern large wind turbines. The prediction code only needs the blade geometry and the turbine operating conditions (wind speed, RPM, blade pitch angle) as input. Previous acoustic array measurements [36–38] showed that broadband trailing edge noise is the dominant noise source for both turbines, which allows a direct validation of the trailing edge noise prediction method. Furthermore, the availability of the array results provides a unique opportunity to assess the prediction code not only in terms of source spectra and overall sound levels as a function of rotor power, but also in terms of the noise source distribution in the rotor plane. Moreover, the predicted directivity and swish amplitude is validated against acoustic measurements on a circle around the turbine, after which the noise and swish 'footprints' of the turbine are calculated.

In order to predict the turbine noise directivity and swish amplitude, the trailing edge noise directivity function must be known. This function was derived before both analytically [4–7,18] and numerically [22]. However, up to now experimental validation of the directivity function was limited to the plane normal to the trailing edge, for directions not too close to the plane of the blade [7,14]. In the present study it is shown that the acoustic measurements on a circle around the turbine in fact constitute a measurement of the *complete* trailing edge noise directivity function, including directions outside the plane normal to the trailing edge and close to the plane of the blade. This feature is used to assess the theoretical predictions of the directivity function against the experimental results.

The organization of this paper is as follows. Section 2 describes the experimental method employed during the field measurements, followed by a description of the prediction method in Section 3. In Section 4 the predictions are validated against the experimental results, and in Section 5 the prediction method is applied to calculate noise and swish footprints around the wind turbine. The conclusions of this study are summarized in Section 6.

2. EXPERIMENTAL METHOD

This section describes the experimental method employed during the field measurements on both turbines. The experimental results are discussed along with the predictions in Section 4. More detailed information about the experimental method can be found in [36–38].

2.1. Test set-up and data acquisition

Acoustic field tests were performed for two different wind turbines. Turbine 1 was a GE 2.3 MW prototype test turbine with a rotor diameter of 94 m and a tower height of 100 m, and was located on a test site in the Wieringermeer polder (Netherlands). Turbine 2 was a

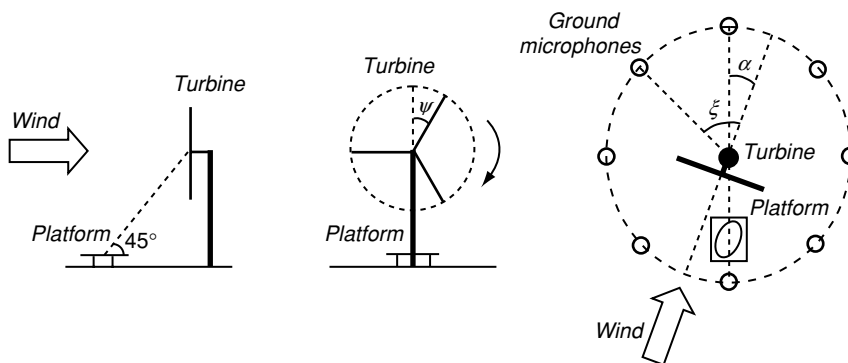**Figure 1:** Test set-up for Turbine 1 (left) and Turbine 2 (right).

Figure 2: Schematic picture of test set-up: side view (left), front view (middle), and top view (right).

GAMESA G58 850 kW turbine with a rotor diameter of 58 m and a tower height of 55 m, and was located on a wind farm in northern Spain. Both turbines were pitch-controlled and rotated in clockwise direction as seen from upwind (Fig. 1). The geometry of the three blades of each turbine was nominally identical. Whereas the blades of Turbine 1 were untreated, for Turbine 2 one blade was cleaned, one blade was tripped, and one blade was untreated, to assess the effect of blade roughness due to for example dirt or insects.

A schematic picture of the test set-up is given in Fig. 2. The source localization measurements were done using a 148-microphone acoustic array, mounted on a

horizontal wooden platform of about 16×18 m^2. The distance between the platform and the tower was roughly the same as the tower height, resulting in a 'view angle' of about 45°. The array microphones (Panasonic WM-61) were mounted flush to the platform and had no wind screens. The array had an elliptic shape to correct for the oblique view angle, and an increased microphone density in the center to reduce coherence loss and ensure low side-lobe levels at high frequencies. In addition to the acoustic array, for Turbine 1 eight ground microphones (LinearX M51) were placed on a 240-m diameter circle around the turbine (with 45°intervals), to measure the directivity of the turbine noise (Fig. 2). The ground microphones were equipped with hemisphere wind screens, and were placed horizontally on a 1-m diameter ground board, with their axes pointing to the turbine [40]. As a reference, an identical microphone, equipped with windscreen, was placed in the center of the array. In Fig. 2, ψ indicates the azimuthal angle of the rotor, α indicates the misalignment angle between turbine and array, and ξ indicates the position of a ground microphone with respect to the downwind direction.

The acoustic signals were measured using a sample frequency of 30.7 kHz (Turbine 1) or 51.2 kHz (Turbine 2) and a measurement time of 30 s. The data were processed using an FFT block size of 1024 (Turbine 1) or 2048 (Turbine 2) with a Hanning window and 50% overlap, yielding a narrowband frequency resolution of 30 Hz for Turbine 1 and 25 Hz for Turbine 2. A second-order 500 Hz high-pass filter was used to extend the dynamic range of the A/D converter. The sound levels were corrected for the filter response and for pressure doubling due to the platform or ground boards. Prior to the measurements, the sensitivity at 1 kHz was determined for all microphones using a calibrated pistonphone. The frequency response was taken from previous calibration measurements for the array microphones and from calibration sheets for the ground microphones. Phase matching of the array microphones was checked using a calibration source at known positions. A trigger signal from the turbine (one pulse per revolution) was recorded synchronously with the acoustic signals, so that the position of the rotor blades was known at all times. In parallel to the acoustic measurements, several turbine and meteo parameters were measured at a sample rate of 3 Hz or higher, including the wind speed, wind direction, turbine orientation, turbine power, RPM, and blade pitch angle. It should be noted that the measured nacelle wind speed for Turbine 2 suffers from an uncertainty. Therefore, in Section 4 the overall sound levels are analyzed as a function of rotor power rather than wind speed.

The test period was 1-15 November 2005 for Turbine 1, and 8-15 December 2003 for Turbine 2. Following the IEC norm for wind turbine noise measurements [40], it was attempted to obtain array measurements for wind speeds (at 10 m height) between 6 and 10 m/s. The wind speed at 10 m height was calculated from the average nacelle wind speed using the standard wind profile from the IEC norm, where the measured nacelle wind speed was assumed to be the free stream wind speed at hub height. On the basis of the turbine operational data, the most stable measurements (i.e. small misalignment angle and small variation in wind speed, RPM, and pitch angle) were selected for further analysis. An overview of the test conditions for the selected measurements is given in Table 1. The ground microphone measurements for Turbine 1 are mentioned separately, because these were all done on the same day.

Table 1: Overview of average test conditions (standard deviation between brackets). The first five columns indicate the number of measurements in the wind speed bins between 6 m/s and 10 m/s (wind speed at 10 m height).

	# meas. per U_{10} bin					U_{nac}		pitch	P	α
	6	**7**	**8**	**9**	**10**	**(m/s)**	**RPM**	**(°)**	**(MW)**	**(°)**
Turbine 1 (array)	14	14	13	5	0	10.3 (1.2)	14.7 (0.3)	0.2 (0.5)	1.6 (0.4)	−2 (3)
Turbine 1 (ground mics)	10	21	15	0	0	10.0 (1.0)	14.6 (0.4)	0.0 (0.0)	1.5 (0.3)	−11 (6)
Turbine 2 (array)	6	6	12	5	6	10.5[*] (1.7)	24.9 (1.9)	−0.1 (0.8)	0.47 (0.19)	−5 (7)

[*]The measured nacelle wind speed for Turbine 2 suffers from an uncertainty.

2.2. Phased array processing

The microphone array data are processed using two different methods. The first method employs conventional beamforming [41] to localize the noise sources in the rotor plane. The resulting source maps show the integrated effect of the three blades, averaged over many revolutions (averaging of spectra was done on energy basis). The calculations are performed in narrow bands and then summed to 1/3-octave bands. The scan grid is placed in the rotor plane, accounting for the misalignment angle α (see Fig. 2) and the rotor tilt angle (i.e. the angle between the rotor axis and the horizontal plane). To improve the resolution and to suppress background noise (for example wind-induced pressure fluctuations on the microphones), the main diagonal of the cross-power matrix (i.e. the auto-powers) is discarded. A frequency-dependent spatial window is applied to the microphone signals, in order to improve the resolution at low frequencies and to suppress coherence loss effects at high frequencies (due to propagation of the sound through the atmospheric boundary layer). The effect of sound convection in the atmospheric boundary layer is taken into account by calculating the average wind speed between rotor and array from the standard wind profile in the IEC norm for wind turbine noise measurements [40]. The noise sources in the rotor plane are quantified using a source power integration method [42]. This technique sums the source powers in (part of) the measured source map, and corrects the results with a scaling factor obtained by performing a simulation for a monopole source at the centre of the integration region. The thus obtained integrated sound pressure level of the turbine is similar to the 'apparent sound power level' defined in [40]. By defining one integration contour around the whole rotor plane and one only around the nacelle, noise levels from the nacelle and the blades are determined.

The second processing method employs three rotating scan planes to produce acoustic source maps for the three individual blades, averaged over a specified azimuth range and over one or more revolutions [43]. The scan planes are placed around the blades, in the rotor plane, and their azimuthal position is determined using the trigger signal from the turbine. For each scan location and each microphone signal, the

dedopplerized source signal is reconstructed by applying a time shift to each sample of the microphone signal. This time shift accounts for the travel time between the (rotating) scan location and the microphone. By summing the reconstructed source signals for all microphones, the acoustic signal emitted from a given scan location is obtained (if no source is present at the scan location the source signals from the different microphones will cancel). The de-dopplerized noise from the blades is quantified using a power integration method for moving sound sources [44], which is similar to the above-mentioned integration method for the rotor plane. An integration contour is defined which includes the noise from the blade but excludes the noise from the nacelle. The thus obtained integrated sound levels represent the contribution of the different blades to the overall sound pressure level of the turbine, as measured at the array position.

The accuracy of the source localization and quantification with the present array set-up was discussed in [38]. With regard to the spatial resolution, the location of a whistle on the blade (at a position unknown to the acoustic test team) was determined within 0.5 m, which is considered to be accurate enough for these tests. Concerning the *relative* sound levels (i.e. differences between the blades), an accuracy of 0.1 dB was found by comparing the average overall blade noise levels for two consecutive revolutions. The accuracy in terms of *absolute* sound levels, which is most relevant for the present study, can be assessed by comparing the integrated rotor source maps to the measured sound level at the reference microphone (with wind screen) in the center of the array. If all the noise measured by the reference microphone is due to the turbine rotor (background noise measurements with stopped rotor indicated a signal-to-noise ratio of 10 dB for the reference microphone), these spectra should coincide. However, for the present measurements on Turbine 1, the average integrated level is found to be 2 dB lower than the level at the reference microphone (this difference is fairly constant as a function of wind speed). This underestimation may be caused by certain simplifications in the integration method and/or by coherence loss at the array microphones, due to the propagation of the sound through the turbulent atmospheric boundary layer. Similar effects have been observed in open jet wind tunnel tests [42] and flight measurements [44]. In Section 4.2 it is shown, by means of the simulated rotor noise source distribution, that the underestimation of the rotor noise level due to the integration method is about 1.4 dB, which suggests that the remaining 0.6 dB is due to coherence loss. Thus, for the assessment of the predicted overall sound levels (Section 4.3), 2 dB is added to the measured rotor noise levels, to account for integration and coherence loss effects.

3. PREDICTION METHOD

Since the field measurements show that broadband trailing edge noise is the dominant noise source for both turbines [36–38], only this noise source is incorporated in the prediction method, which means that inflow-turbulence noise, blunt trailing edge noise, and tip noise are discarded. The calculation can be divided into three steps: blade aerodynamics (Section 3.1), trailing edge noise source strength (Section 3.2), and directivity and convective amplification (Section 3.3). The resulting rotor noise source distribution can then be used to calculate simulated acoustic source maps or noise footprints around the turbine (Section 3.4).

3.1. Blade aerodynamics

For the aerodynamic calculations the blade is first divided into a number of radial segments (21 for both turbines in the present study). Next, for each segment the local Reynolds number and angle of attack are obtained from an aerodynamic wind turbine model, based on the blade element momentum theory [45]. Then, the RFOIL airfoil design and analysis code [46] is used to calculate the trailing edge boundary layer displacement thicknesses on the pressure and the suction side. RFOIL is an extension of XFOIL [47] and takes into account rotational effects.

As input to the aerodynamic calculations only the blade geometry and the turbine operating conditions are needed. The blade geometry (including the airfoils) for both turbines was provided by the manufacturers, and the RPM and blade pitch angle were taken according to the turbine control system, as measured during the field tests. The aerodynamic profile coefficients (c_l, c_d, and c_m as a function of angle of attack) for Turbine 1 were supplied by the manufacturer. For Turbine 2 they were obtained from the Aerodynamic Table Generator [48], which contains a large database of airfoil characteristics measured under 2D conditions in the wind tunnel.

The effects of atmospheric turbulence, wind shear, and yaw are neglected in the calculations, i.e. stationary and axisymmetric conditions are assumed. Furthermore, it is assumed that the airfoils are clean (i.e. free transition), because the clean rotor is considered to be most representative for normal operation [38]. Thus, for Turbine 1 (which has untreated blades) the calculations can be directly compared to the experimental results. For Turbine 2 (which has one clean, one tripped, and one untreated blade), the measured data must be corrected to obtain the noise from a 'clean' rotor (see Sections 4.2 and 4.3). The trip option in XFOIL is not used because this may not be representative for the trips applied in the field tests.

In the present study calculations are done at wind speeds between about 5 m/s and 12 m/s, in steps of 0.5 m/s. The calculated displacement thickness as a function of radius is shown for both turbines in Fig. 3. These results represent conditions close to the average experimental conditions, i.e. wind speeds of 9.75 and 8.75 m/s, RPM values of 14.75 and 25.8, and pitch angles of 0.04° and 0.1° for Turbine 1 and Turbine 2, respectively. The quality of the aerodynamic modelling was verified by comparing the calculated and measured power curve for Turbine 1, and generally good agreement was found. It should be noted that this agreement does not guarantee that the calculated boundary layer thickness is correct. However, for the present field tests more detailed experimental information about the blade aerodynamics is not available. For Turbine 2 a comparison between the measured and calculated power curve is not possible, due to an uncertainty in the wind speed measurements. Thus, in order to avoid disturbing effects from uncertainties in the measured wind speed, in Section 4 the overall sound levels are plotted as a function of rotor power rather than wind speed.

3.2. Trailing edge noise source strength

Using the boundary layer displacement thickness and local Reynolds number from the previous section as input, the source spectrum for each radial blade segment is calculated using the 2D semi-empirical trailing edge noise prediction code developed by
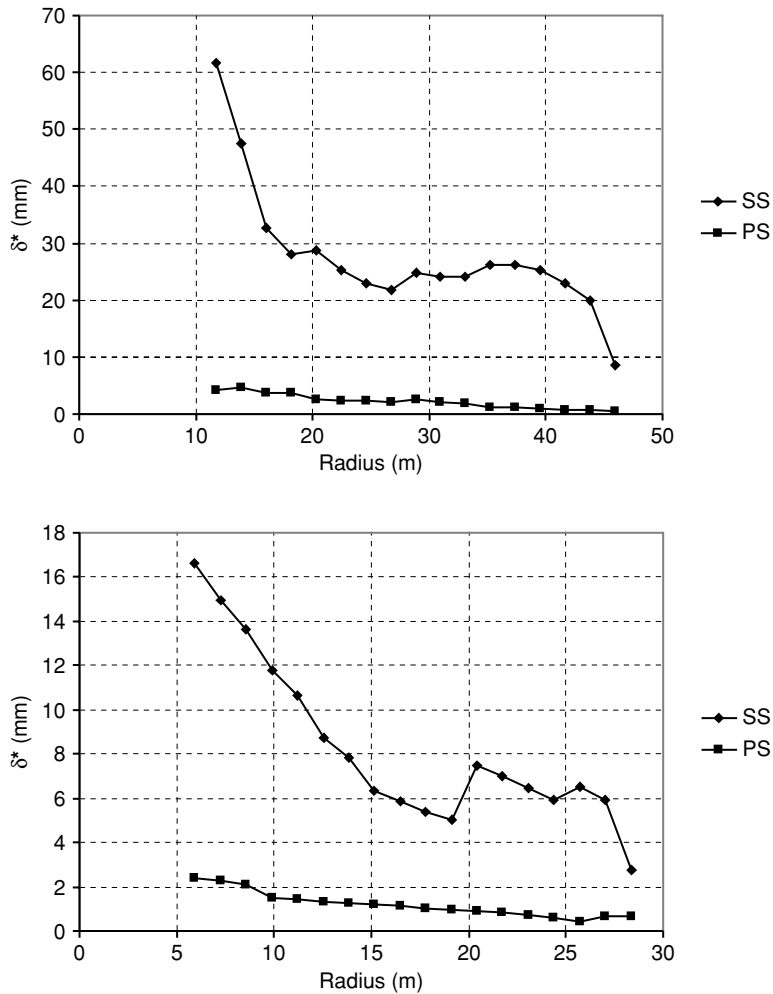
Figure 3: Calculated trailing edge boundary layer displacement thickness on pressure and suction side, for Turbine 1 (top) and Turbine 2(bottom).

Brooks, Pope, and Marcolini [9]. In this code, the total trailing edge source strength due to the turbulent boundary layer is the sum of three contributions of the following form:

$$SPL_i = 10\log\left(\frac{\delta_i^* \, M^5 L}{r^2}\right) + A_i\left(\frac{St_i}{Sr_i}\right) + K_i \tag{1}$$

where δ^* is the displacement thickness, M the Mach number, L the span of the blade segment, r the distance to the observer, and K an empirical constant which depends on

13

the Mach and Reynolds numbers. The function *A* describes the spectral shape as a function of the ratio between the Strouhal number $St = f \cdot \delta^*/U$ (with *U* the local flow speed) and the empirical peak Strouhal number *Sr*. The three contributions (here denoted by the index *i*) are the pressure side boundary layer, the suction side boundary layer, and an additional contribution to account for nonzero angle of attack. Eq. (1) is based on theoretical analyses of a turbulent, low Mach number flow over a half-plane [4], and basically states that trailing edge noise scales with the boundary layer thickness (which is a measure for the turbulence correlation scale) and the fifth power of the flow speed. The dependence on U^5 was confirmed in many experimental studies, and was also found for the trailing edge noise from the present turbines [36]. Note that Eq. (1) only calculates the source strength for an observer at a fixed position with respect to the blade segment; directivity and convective effects are discussed in the next section.

For the trailing edge noise calculations in the present study, the original Fortran code from [9] is used with only two modifications. The first modification is that we use (for each blade segment) the trailing edge boundary layer thickness as calculated in the previous section, instead of the boundary layer thickness calculated by the program (which is an estimate for a NACA0012 airfoil). The second modification is as follows. In the original code, Eq. (1) takes a different form for angles of attack larger than the 'stall angle' of 12.5°. In the present calculations the stall angle is adjusted to the actual stall angle for the different airfoils, which is known from 2D wind tunnel measurements. However, since these stall angles are never reached for radii larger than 30% of the tip radius, effectively only Eq. (1) is used for the present predictions, with all empirical constants according to [9].

3.3. Directivity and convective amplification

The calculation in the previous section yields the trailing edge source spectrum in 1/3-octave bands, for each radial blade segment. In order to obtain the *effective* source strength for a given blade azimuth angle, as perceived by an observer at a specified position, the effects of trailing edge noise directivity and convective amplification should be taken into account. Amiet [5] derived an analytical expression for the directivity of trailing edge noise from a flat plate of arbitrary chord (see Fig. 4 for definition of angles). Fig. 5 shows the characteristics of this theoretical directivity function for a number of nondimensional frequencies, in the plane normal to the trailing edge (in terms of the acoustic pressure *p*), and on a sphere around the trailing edge source (in dB). In these figures the flow is in the *x*-direction and the trailing edge runs along the *y*-axis. For low frequencies (i.e. small C/λ, with *C* the blade chord and λ the acoustic wavelength), the directivity shows the classical dipole pattern with $p^2 \sim \sin^2(\theta_A) \cdot \sin^2(\varphi_A)$, while for high frequencies (large C/λ) the cardoid pattern $p^2 \sim \sin^2(\theta_A/2)$ is found in the plane normal to the trailing edge. The directivity function for high frequencies is equivalent to that obtained by Ffowcs Williams and Hall [4] and Howe [6], who used an alternative theoretical approach and found $p^2 \sim \sin^2(\theta_H/2) \cdot \sin(\varphi_H)$. For intermediate frequencies more complicated patterns with multiple directivity lobes are obtained [see also 12,13]. The effect of a leading edge back-scattering correction to Amiet's formulation was investigated by Roger and Moreau [18], but they found this correction to be negligible for large wind turbine blades.
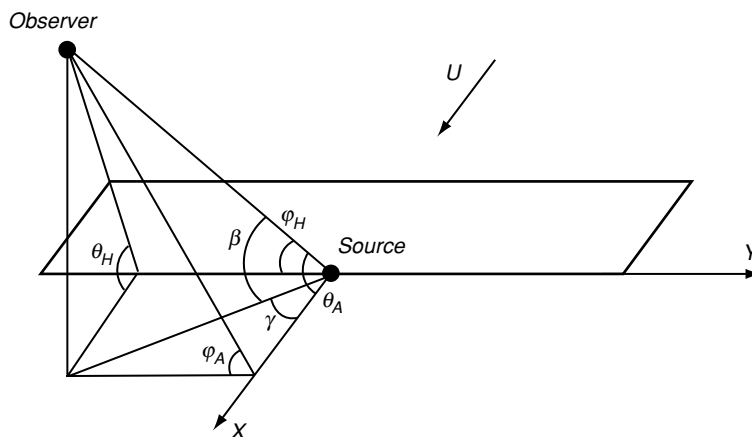
Figure 4:   Definition of angles between observer and trailing edge source.

For the present turbines, C/λ is roughly between 0.4 and 4 for the relevant blade radii and frequencies. In order to assess the influence of the trailing edge noise directivity function on the wind turbine noise directivity and swish amplitude, it is useful to know the position of an observer on the 'directivity sphere'. For this purpose, the 'trajectories' of the eight experimental ground microphones on the directivity sphere, during one revolution of the blade, are projected on the high-frequency directivity function in Fig. 6 (a source radius of 0.9 times the tip radius is used). It can be seen that each ground microphone follows a circle at more or less constant 'latitude' β, where β depends on the microphone angle ξ (the 'longitude' γ depends on the blade azimuth angle ψ). The four lower circles represent the upwind locations, while the four upper circles correspond to the downwind locations. The asymmetry between the upper and lower trajectories is due to the rotor tilt angle, the blade pitch and twist, and the average experimental misalignment angle α of $-11°$. For a symmetrical turbine (i.e. no pitch, twist, and tilt), the latitude of an observer at large distance would be given by $\beta = |\xi - \pi| - \pi/2$. Fig. 6 illustrates that the directivity measured by the farfield microphones is determined by the *average* level over each trajectory, while the swish amplitude depends on the *variation* of the level along each circle (note that there are three blades on each circle, the contributions of which should be summed). Thus, the ground microphone measurements on a circle around the turbine in fact constitute a measurement of the complete trailing edge noise directivity function, and, vice versa, in order to predict the noise footprint of a wind turbine, the complete directivity function should be known.

The dependence of the wind turbine noise directivity and swish amplitude on the trailing edge noise directivity function can be exploited to assess the theoretical diectivity function against the experimental results. First, the exact, frequency-dependent theoretical flat plate directivity function (Fig. 5) is considered. The resulting turbine noise and swish directivity are shown in Fig. 7 ('exact'), and show reduced levels and high swish amplitudes for positions close to the rotor plane. These trends
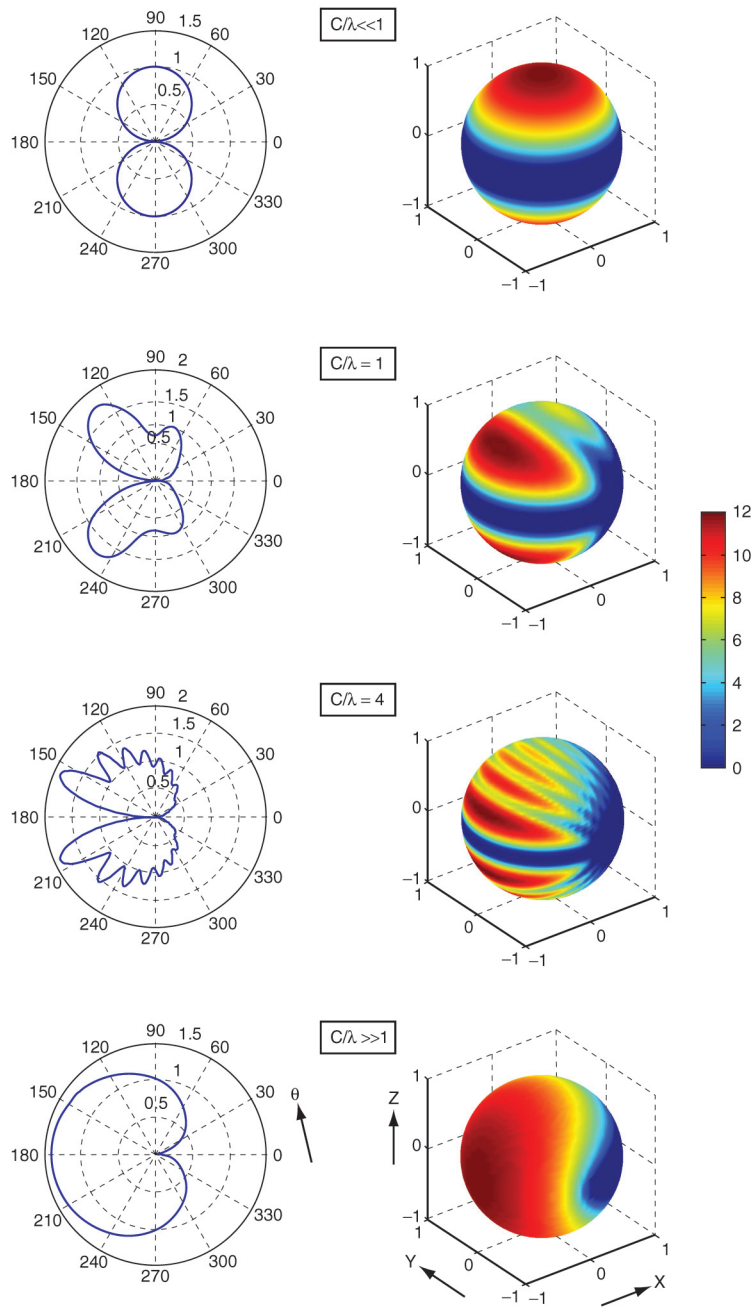
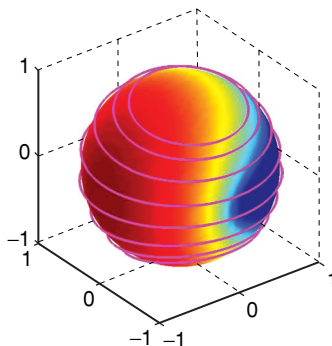**Figure 5:** Theoretical trailing edge noise directivity function for flat plate [5].

16

Figure 6: Theoretical high-frequency trailing edge noise directivity function with 'trajectories' of ground microphones: $\xi = -11°$, 34°, 304°, 79°, 259°, 124°, 214°, 169° (top to bottom).

agree well with the experimental results (to be discussed in Section 4.4), but due to the steep fall-off of the directivity function for small β (Fig. 5), relatively large quantitative deviations are found close to the rotor plane. Next, the high-frequency directivity function $p^2 \sim \sin^2(\theta_H/2) \cdot \sin(\varphi_H)$ (Fig. 6) is considered. However, although these predictions (Fig. 7, 'HF') also show increased swish amplitudes close to the rotor plane, the experimental 'dips' in the directivity (around $\xi = 90°$ and $\xi = 270°$) are not reproduced. Therefore, a frequency-independent directivity function is defined, which shows good agreement with the measurements for all directions, and allows easy implementation in prediction codes. The basis of this directivity function is a modified version [9] of the theoretical high-frequency trailing edge noise directivity: $p^2 \sim \sin^2(\theta_A/2) \cdot \sin^2(\varphi_A)$. This function (Fig. 8A) has the cardoid pattern in the plane normal to the trailing edge, and shows the desired fall-off to zero in the plane of the blade, by assuming that the φ-dependence is the same as for the classical low-frequency dipole [49]. In previous studies it was used for the prediction of noise from helicopters [50] and wind turbines [24, 26, 30–32], and in [36, 37] it was succesfully applied to explain the rotor noise source distribution as perceived at an upwind observer position. However, this function has a discontinuity for $\theta_A = \pi$, causing unrealistically high swish amplitudes close to the rotor plane (Fig. 7, 'BPM'). Therefore, the function is smoothed around the discontinuity by averaging it over a certain range of β and γ. On the basis of the experimental results, the averaging range $(d\beta, d\gamma)$ is chosen to be $(\pi/12, 2\pi/3)$ for $\beta = 0°$, and is reduced to $(0, 0)$ for $\beta = \pi/2$ (using the error function). Thus, for regions away from the plane of the blade, the smoothed function is identical to the original function used in [9]. The resulting turbine noise directivity and swish amplitude (Fig. 7, 'BPMs') correspond well to the experimental results (Section 4.4). Thus, this smoothed, semi-empirical directivity function (Fig. 8B) appears to be a good approximation of the true directivity function for trailing edge from an airfoil. It shows similar characteristics as the theoretical directivity function in Fig. 5 ($C/\lambda = 1.4$), except for the steep fall-off close to the plane of the blade ($\beta = 0°$).
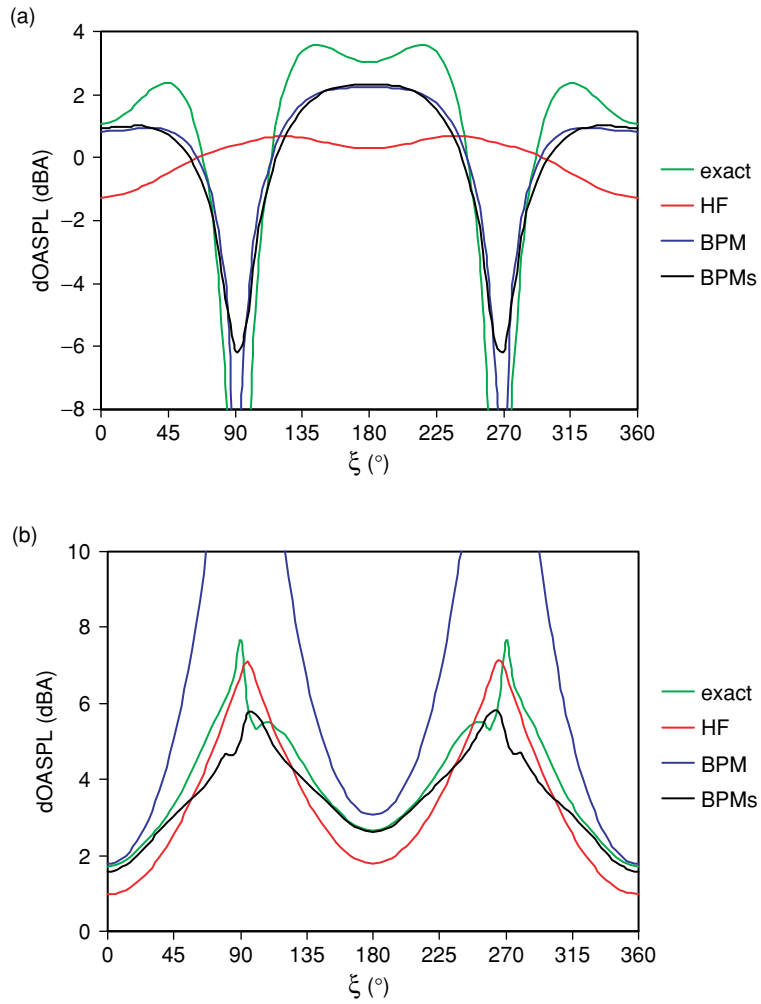
(a)

(b)

Figure 7: Predicted turbine noise directivity (a) and swish amplitude (b) for four different trailing edge noise directivity functions.

Thus, for the present predictions the following function is used to account for directivity and convective amplification:

$$D_s = \frac{\left[2\sin^2\left(\theta_A/2\right)\sin^2\varphi_A\right]_s}{\left(1 - M\cos\xi\right)^4}, \tag{2}$$

18
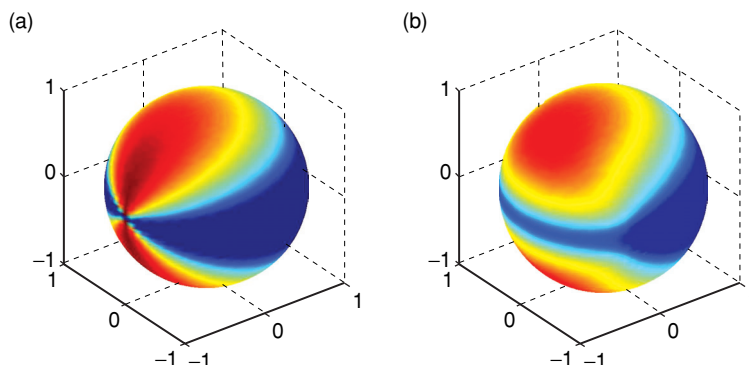
Figure 8: (a) Analytical trailing edge noise directivity function [9]. (b) Smoothed analytical directivity function used in present prediction code.

where the subscript s indicates the smoothing over β and γ, ξ is the angle between the blade flow velocity and the source-observer line, and M is the (undisturbed) blade Mach number. The numerator in Eq. (2) describes the trailing edge noise directivity as discussed above, and is the most important contributor to the asymmetrical rotor noise source pattern [36]. The denominator represents the convective amplification factor for trailing edge noise, and indicates that the source amplitude increases when the source is moving towards the observer. As mentioned by Brooks and Burley [50], different exponent power laws between 1.5 and 4.5 have been found in different theoretical approaches, while experimental validation has been very limited. Following [50], here the 4th power for compact dipole sources is used [51]. For the present low Mach numbers this convective factor is practically equivalent to that derived by Howe [6] for trailing edge noise. The Doppler *frequency* shift is accounted for by calculating for each source frequency the Doppler-shifted frequency at the observer position, and redistributing the acoustic energy over the appropriate frequency bands.

3.4. Simulated source maps and noise footprints

From the effective radial source strength distribution (for a given blade azimuth and observer position), as determined in the previous section, acoustic source maps and turbine noise footprints are calculated as follows. For the source maps, first the average noise source distribution in the (tilted) rotor plane is predicted, for an observer position corresponding to the position of the microphone array in the experiments. This is done by dividing one complete revolution in 180 azimuthal blade positions (i.e. an azimuthal interval of 2°), and calculating for each blade position the effective radial source distribution. In order to obtain the *average* source level for each azimuthal position, the source powers are divided by the total number of azimuthal blade positions (180). Since the number of *radial* segments is 21, the resulting rotor source distribution is composed of 3780 incoherent sources, each with a Doppler-shifted 1/3-octave band spectrum

which includes directivity and convective effects. Using this source distribution, the acoustic signals (complex amplitude as function of narrowband frequency) are calculated for all microphone positions in the array, from which a simulated cross-power matrix is constructed. This cross-power matrix is further processed using the same procedure that is used for the measured data (see Section 2.2), allowing direct comparison to the experimental results.

For the noise footprints, three blades are modeled at 120° from each other. The radial source distribution for each blade is calculated as described in the previous section. Thus, for a given rotor position, the total number of sources is 63. The revolution is divided in 72 azimuthal rotor positions (i.e. an interval of 5°), and for each rotor azimuth the contribution of each blade segment to the sound level at a certain observer position is calculated. For a given *emission* time (i.e. emission azimuth), the *arrival* time is generally different for the 63 blade elements. Thus, in order to calculate the perceived sound level at a fixed arrival- or *observer* time, the contribution of each blade segment is determined by interpolation between two emission azimuths. By plotting the total sound level at different observer positions for a fixed observer time, the instantaneous noise footprint is obtained. The observer time can also be expressed in terms of the rotor azimuth at observer time. By calculating noise footprints for a complete revolution (in steps of 5° azimuth), a 'time history' is obtained for each observer position. The swish amplitude for a given observer position is calculated as the difference between the minimum and maximum perceived sound level during one revolution. In the predictions a uniform wind speed is incorporated to account for convection of sound, but refraction due to wind shear is not included.

4. COMPARISON BETWEEN PREDICTION AND EXPERIMENT

In this section the predictions are compared to the experimental results. This assessment is made in terms of the noise source distribution in the rotor plane (Section 4.1), the rotor noise spectra (Section 4.2), the overall sound level as a function of rotor power (Section 4.3), and the directivity and swish (Section 4.4).

4.1. Noise source distribution in rotor plane

The measured and predicted source maps for both turbines are shown in Fig. 9 to Fig. 12 (details of the simulations are provided in Section 3.4). Note that these source maps correspond to the upwind measurement position on the ground. The range of the colour scale is always 12 dB, and the maximum is adjusted for each individual frequency band. The turbines rotate in clockwise direction and the black circle indicates the trajectory of the blade tips. The experimental source maps are averaged over all measurements, the simulations are done for a misalignment angle of 0° and turbine conditions close to the average experimental conditions (see Section 3.1).

In general good qualitative agreement is observed between experiments and simulations. As in the experiments, the simulated source maps show dominant noise radiation from the outer part of the blades, during their downward movement. This asymmetric source pattern, which is due to trailing edge noise directivity and convective amplification, causes the swishing noise during the passage of the blades. Note that for
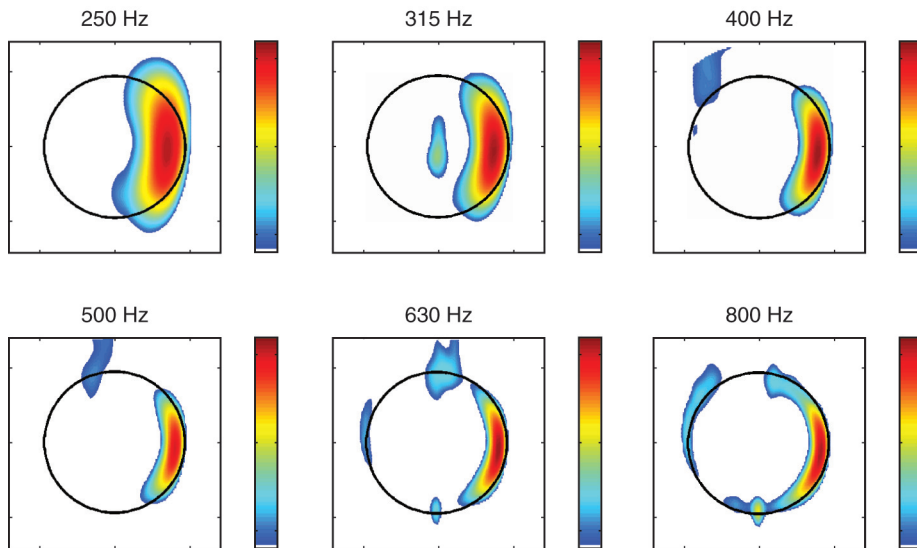
250 Hz 315 Hz 400 Hz

500 Hz 630 Hz 800 Hz

Figure 9: Measured source maps for Turbine 1.
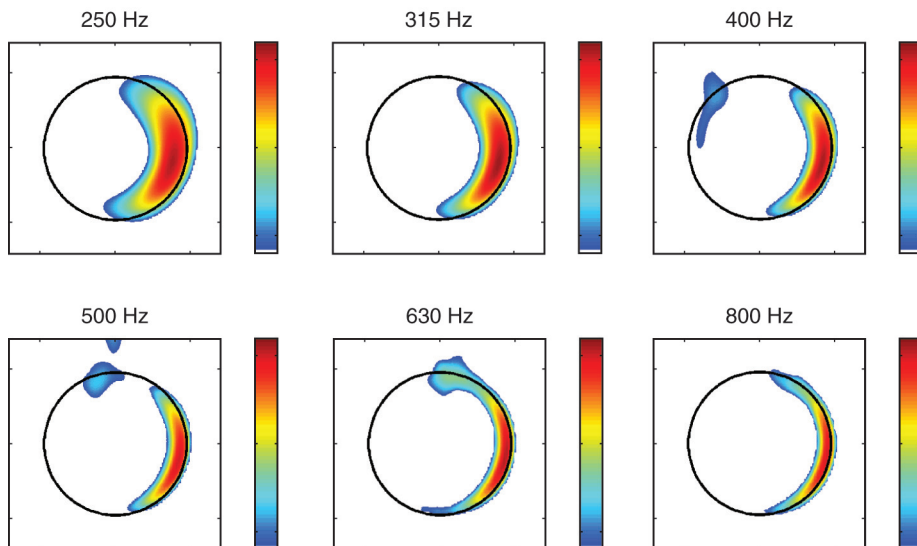
250 Hz 315 Hz 400 Hz

500 Hz 630 Hz 800 Hz

Figure 10: Predicted source maps for Turbine 1.

an observer on the ground, due to the time delay between emission and perception of the sound, the swish may *seem* to be generated when the blades are close to the tower (depending on RPM and distance to the turbine). Similar to the experiments, the predicted source maximum shifts to a higher radius for increasing frequency, which can
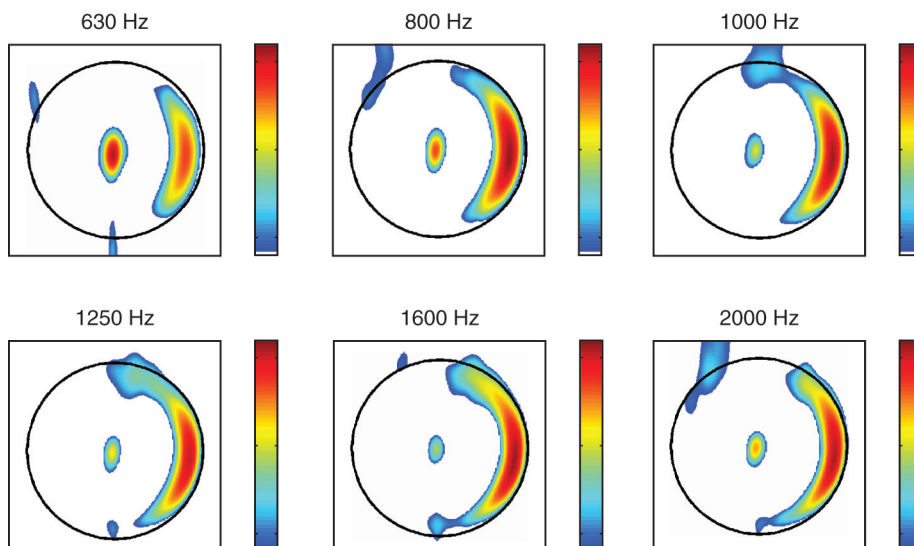
Figure 11: Measured source maps for Turbine 2.
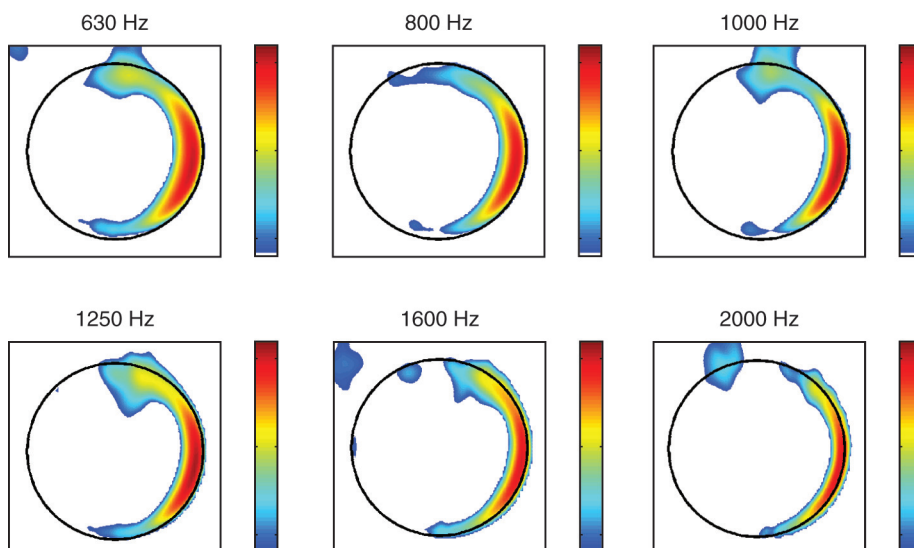
Figure 12: Predicted source maps for Turbine 2.

be attributed to the higher flow speed and thinner trailing edge boundary layer. In some cases even the minor side-lobes (for example between 10 and 12 o'clock for 400–630 Hz in the Turbine 1 results), which are an artefact of the array method, are reproduced in the simulations. Obviously, the minor experimental noise sources at the nacelle and the
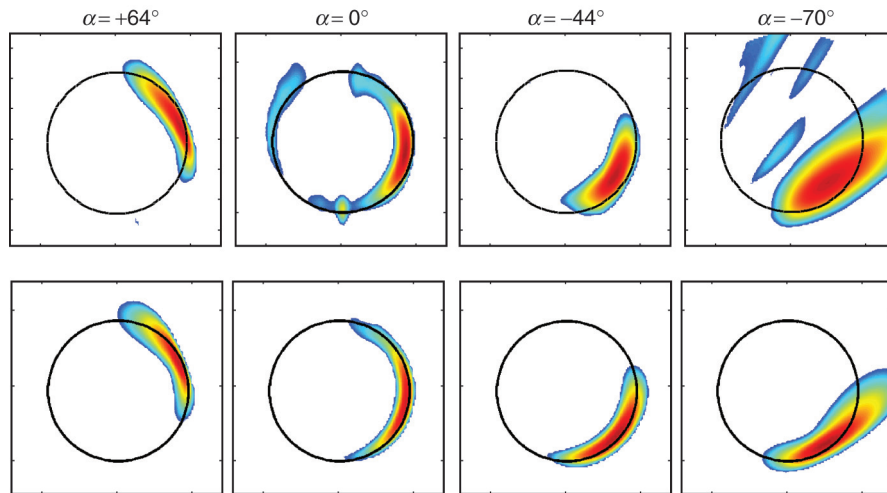
$\alpha= +64°$ $\qquad$ $\alpha= 0°$ $\qquad$ $\alpha= -44°$ $\qquad$ $\alpha= -70°$

Figure 13: Measured (upper row) and predicted (lower row) source maps for Turbine 1 at different misalignment angles (800 Hz).

tower are not reproduced in the simulation, because these are not simulated in the trailing edge noise prediction model. The nature of the 'tower source', which occurs at higher frequencies for both turbines, is hard to assess on the basis of the present data, but it could originate from (1) reflection of blade noise on the tower, (2) impingement of blade tip vortices on the tower, and/or (3) the upstream influence of the tower on the flow field around the blade. At high frequencies, Turbine 1 also shows a minor tip noise source during the upward movement of the blades, which is not modeled in the present prediction model.

Whereas the previous results concern misalignment angles around 0°, for Turbine 1 experimental data are also available for large misalignment angles. The measured and predicted source maps for these angles are shown in Fig. 13. It can be seen that the location of the source region shifts upward or downward when the right- or left-hand side of the rotor plane is turned towards the array, respectively. This can be qualitatively explained by the change in the component of the blade velocity in the direction of the array, which results in a change in convective amplification (Section 3.3). At high misalignment angles the array resolution decreases due to the oblique view angle. Again a good qualitative agreement between simulation and experiment is found, indicating that the changes in source pattern are well captured by the trailing edge noise prediction method.

4.2. Rotor noise spectra

As explained in Section 2.2, the source maps are quantified using a power integration method. Before comparing the predictions to the measured rotor noise spectra, first some intermediate results from the predictions are discussed. As an example, Fig. 14 shows three rotor noise spectra from the simulations for Turbine 1: the source strength spectrum (output of Section 3.2), the rotor spectrum after including directivity and
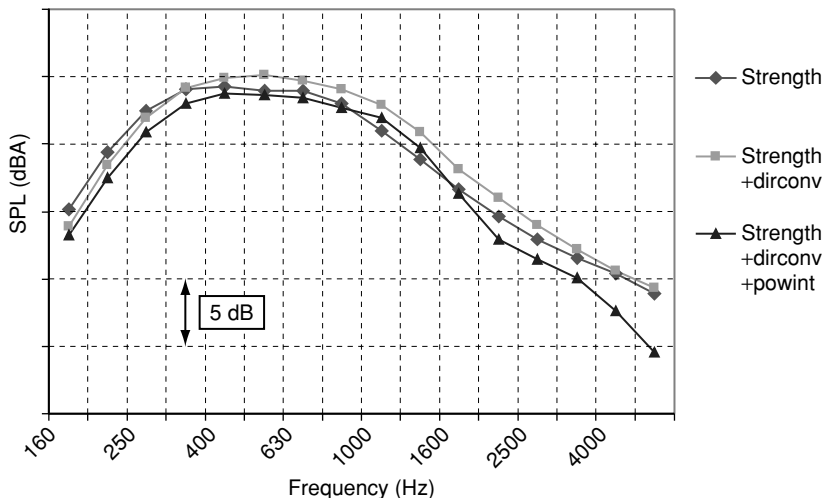
Figure 14: Intermediate rotor noise spectra from the prediction for Turbine 1.

convective effects (Section 3.3), and the integrated rotor spectrum from the array simulation (Section 3.4). By comparing the first two lines, it can be seen that directivity and convection result in a small shift of the spectrum to higher frequencies, because the blades are moving towards the observer on the ground when they produce most of their noise. Interestingly, the noise *level* is hardly affected: although directivity and convection yield a large asymmetry in the noise source distribution, the effect is rather small when averaged over all rotor azimuths (for the upwind array position). By comparing the second and third line, it can be seen that the power integration method results in an underestimation of the actual rotor noise level. The difference is small at low frequencies, but increases to almost 5 dB at the highest frequency. As mentioned in Section 2.2, this deviation is probably due to certain assumptions and simplifications in the power integration method [42]. As a result of the deviation, the power integration method underestimates the actual overall rotor source level by 1.4 dB for the present simulation. Note that this effect occurs both for the simulated and the measured integrated rotor noise spectra.

The measured and simulated integrated rotor noise spectra for both turbines are shown in Fig. 15 and Fig. 16. These spectra correspond to the source maps presented in Fig. 9 to Fig. 12. As mentioned before, the experimental results are averaged over all measurements, and the simulations are done for turbine conditions close to the average experimental conditions. For Turbine 2 the experimental spectrum is corrected on the basis of the individual blade noise spectra [36], to obtain the spectrum of a 'clean' rotor. For the measured source maps the hub region is excluded from the integration. For both turbines a good agreement between predicted and measured peak frequencies is observed, and the fair prediction of the spectral shape confirms that our model for trailing edge noise is adequate. A quantitative assessment of the predicted overall sound levels is given in the next section.
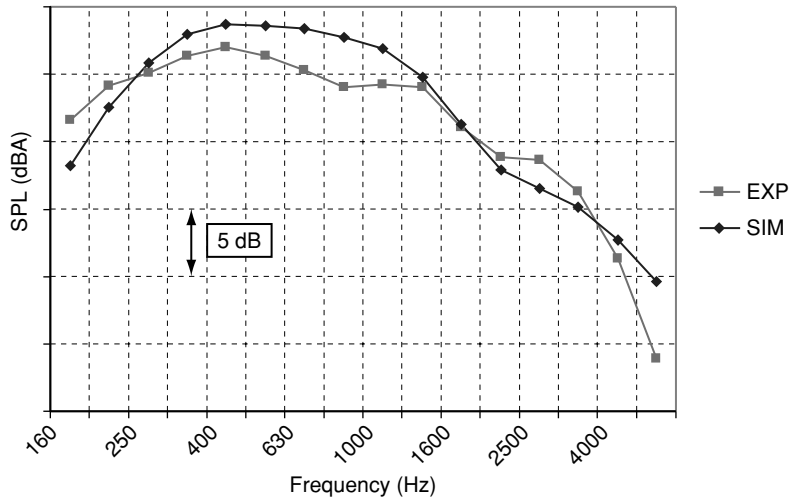
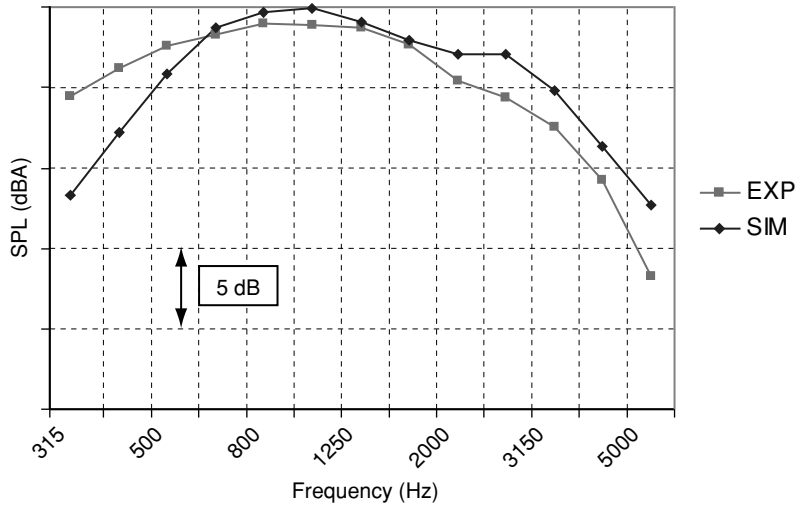**Figure 15:** Measured and predicted rotor noise spectra for Turbine 1.

Figure 16: Measured and predicted rotor noise spectra for Turbine 2.

4.3. Overall sound level as function of rotor power

The results of the previous section show that the average experimental spectra for both turbines correspond well to the predictions for the average experimental wind speed. Next, it is investigated if the predictions also accurately capture the dependence of the turbine noise on wind speed. Calculations are done for a range of wind speeds and the overall sound level is determined as the sum of the predicted rotor source distribution (i.e. without array processing, see Section 3.4). The experimental sound level is determined from the
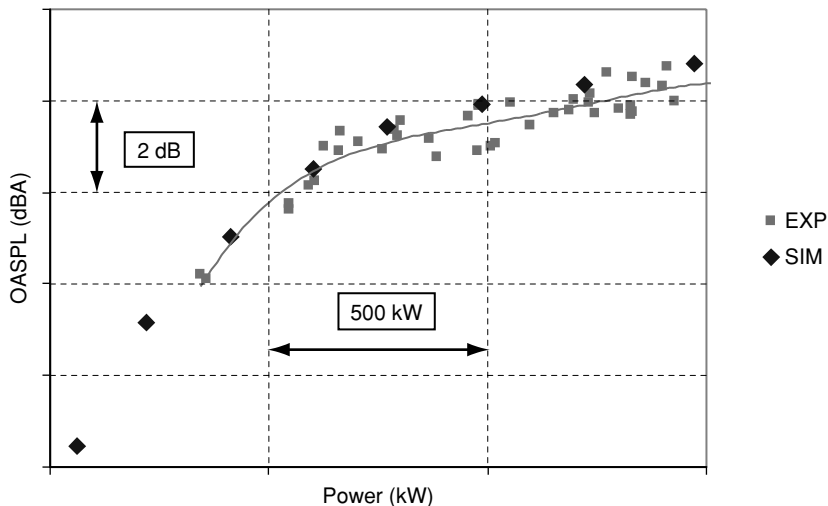
Figure 17:   Measured and predicted overall rotor noise levels for Turbine 1.
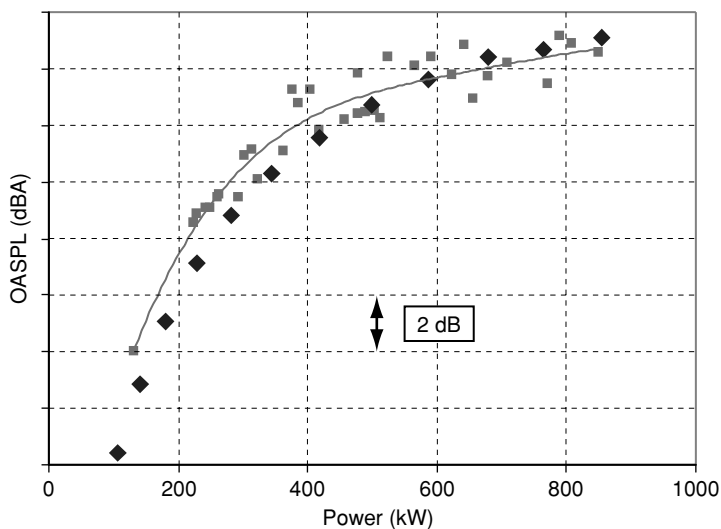

Figure 18:   Measured and predicted overall rotor noise levels for Turbine 2.

integrated rotor spectrum for all measurements, to which 2 dB is added for both turbines to account for the underestimation by the power integration method and coherence loss effects (Section 2.2). In addition, 1.5 dB is subtracted from the overall levels of Turbine 2, to account for the fact that the rotor has a tripped and an untreated blade, while the simulations are for a clean rotor. This 1.5 dB correction is based on the differences in overall sound level between the three blades, which are practically independent of rotor
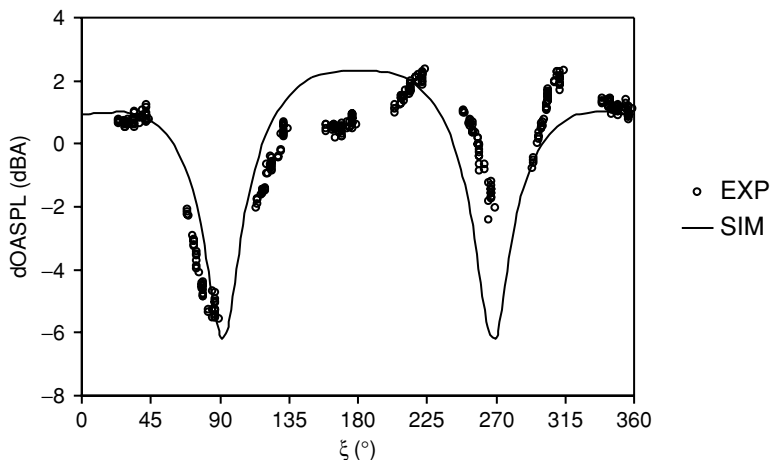
Figure 19: Measured and predicted directivity for Turbine 1.

power [36]. As mentioned in Section 3.1, we focus on the clean rotor since this is considered to be most representative for normal operation. In order to avoid disturbing effects from the uncertainty in the measured nacelle wind speed for Turbine 2, the sound levels are plotted as a function of the rotor power. Fig. 17 and Fig. 18 show that for both turbines a good agreement is obtained between the predicted and measured overall levels. The dependence on rotor power is also well reproduced, although Turbine 2 shows a systematic deviation of 1-2 dB below 500 kW, for which no explanation is available yet. Nevertheless, for both turbines the difference between measurement and prediction is less than 1-2 dB, which is smaller than the scatter in the experimental data. This accuracy is considered satisfactory for the present semi-empirical prediction model.

4.4. Directivity and swish

For Turbine 1, farfield measurements were performed with eight ground microphones on a 240-m diameter circle around the turbine (Fig. 2 and Table 1). To determine the directivity of the turbine noise, the average level on each microphone is plotted as a function of microphone angle ξ for each 30 s measurement (Fig. 19). In order to focus on the dominant trailing edge noise, and exclude possible low-frequency wind noise or high-frequency tip noise, the overall A-weighted levels are summed between 250 and 800 Hz. In order to account for variations in the absolute sound level (due to variations in weather and turbine operating conditions), the levels for each measurement are normalized using the average level on the eight microphones. The average misalignment angle α for the ground microphone measurements is $-11°$, and the variation in α is 20°, which explains the eight 'traces' in Fig. 19. The most distinct feature in the measured directivity pattern are the two 'dips' in the crosswind direction. A similar decrease in noise level close to the rotor plane was also found in [26, 29]. Fig. 19 also shows the *predicted* directivity on a 240-m diameter circle around the turbine, for a wind speed close to the average
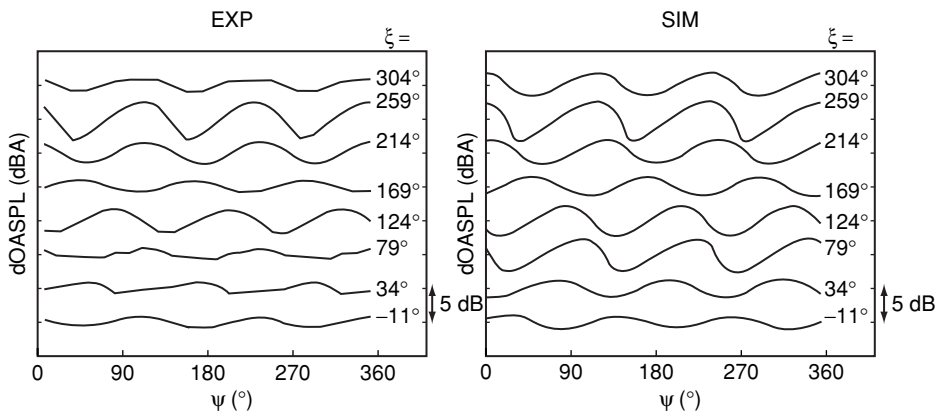
Figure 20: Measured and predicted sound level variation as a function of rotor azimuth ψ, for different farfield positions ξ.

experimental wind speed. It can be seen that the predicted curve follows the measured curve within 1-2 dB, with two 6 dB dips in the cross-wind direction. These dips can be understood from the reduced levels of the trailing edge noise directivity function close to the plane of blade (Fig. 8B). The predicted upwind sound levels are slightly higher than the downwind levels, which is mainly due to the convective factor in Eq. (2), because around $\psi = 90°$ the inverted blade flow velocity vector points slightly upwind.

Next, the *variation* in noise level due to the revolution of the blades (swish) is considered for the different directions. In order to exclude variations due to varying weather or turbine conditions, the overall level on each ground microphone is plotted as a function of the rotor azimuth angle and averaged over all measurements (Fig. 20). For each ground microphone three practically identical humps are found, corresponding to the passage of the blades. The predicted graphs are shown in the same figure. For the upwind measurement positions ($90° < \xi < 270°$), both the amplitude and the phase of the humps match quite well with the measurements. However, for the downwind microphones the measured amplitude is lower than predicted. Since the signal-to-noise ratio (i.e. the minimum sound level in Fig. 20 minus the background noise level with stopped rotor) is generally higher than 9 dB, this does not explain the reduced swish amplitude. However, comparison of the graphs for the individual 30-s measurements (not shown) indicates that slight variations in the phase of the humps reduces the amplitude of the averaged graphs. Due to propagation of the sound through the rotor wake, this effect can be expected to be stronger for the downwind microphones. Thus, in order to obtain a reliable experimental value of the swish, rather than taking the amplitude from the averaged graphs in Fig. 20, the amplitude is determined for each individual 30-s measurement, and then averaged over all measurements. The resulting experimental swish amplitudes are shown together with the predicted values in Fig. 21. The error bars indicate the standard deviation in swish amplitude and farfield position. It can be seen that the swish amplitude is predicted within 1 dB for all directions.
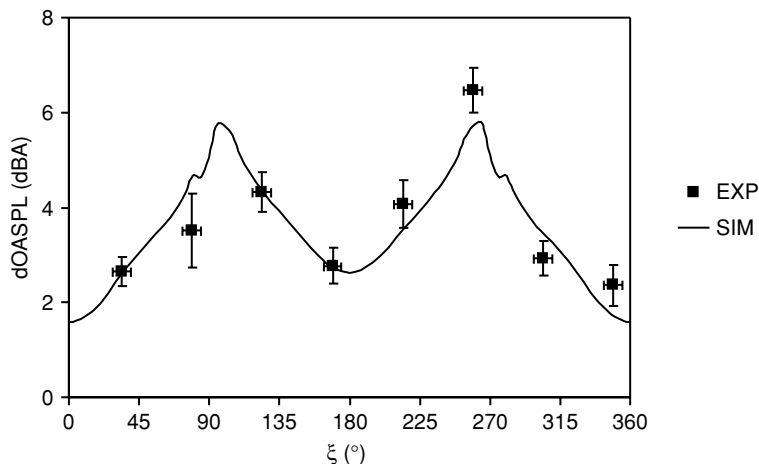
Figure 21: Measured and predicted swish amplitude as a function of farfield position ξ.

The relatively low swish amplitude for $\xi = 79°$ may be partly explained by shielding of the tower [33, 39]. Note that the predicted swish amplitude is closely related to the variation in level along the microphone 'trajectories' (Fig. 6) on the trailing edge noise directivity function in Fig. 8B.

5. APPLICATION: PREDICTION OF NOISE AND SWISH FOOTPRINTS

The previous section provides an extensive validation of the prediction model against the experimental results, in terms of the noise source distribution, rotor noise spectra, wind speed dependence, directivity and swish. The measurements are limited to the array position and a 240-m diameter circle around the turbine. However, since the measurements on the circle cover almost the complete trailing edge noise directivity function (Fig. 6), the prediction method can also be applied to calculate the noise at larger distances. Fig. 22 shows instantaneous turbine noise footprints (top view) for four different rotor azimuth angles, up to a distance of ten times the rotor diameter (details of the calculation are provided in Section 3.4). The turbine is located at the center of the footprint, and the wind goes from left to right. The rotor azimuth at observer time is indicated in the upper right corner of each footprint. In order to limit the range of the dB scale, the levels are normalized using the horizontal distance r_h to the turbine: $SPL_{norm} = SPL + 20 \cdot \log(r_h)$. In this way the levels at a given distance can be directly compared. Note that atmospheric attenuation and sound refraction due to wind shear are not included in the predictions. Refraction may in practice reduce the upwind sound levels.

The footprints show two 'waves' of increased sound level, one in each cross-wind direction, which start close to the turbine at $\psi = 90°$ and propagate outward with the speed of sound. The wave on the side of the down-going blade is generated when the blade is around $\psi = 30°$, while the wave on the side of the upgoing blade is generated
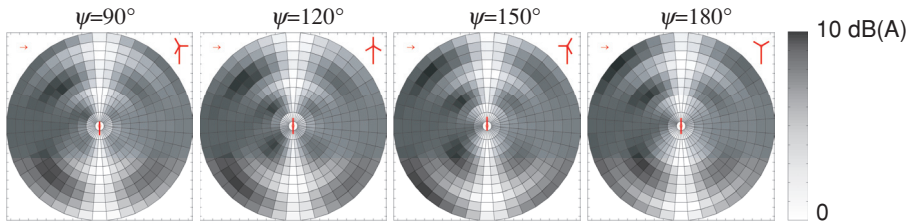
Figure 22: Predicted instantaneous noise footprints for increasing rotor azimuth angle, up to a distance of 10 times the rotor diameter. The wind goes from left to right.
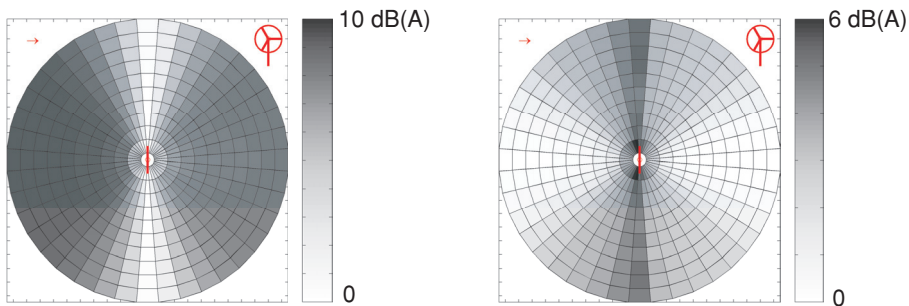

Figure 23: Predicted average footprint (left) and swish footprint (right) for a complete revolution.

when the blade is around $\psi = 180°$. After $\psi = 180°$ the cycle repeats and both waves can be seen to propagate further to the edge of the footprints. The distance between two successive waves is about 5 rotor diameters, which is consistent with the time period of 1.33 s between the passage of two blades (the RPM is 15) and a speed of sound of 340 m/s. Due to the passage of these sound waves from the blades, the noise levels in the crosswind directions vary significantly, while in the up- and downwind directions the levels are quite constant at large distances. This is illustrated in Fig. 23, which shows the average and swish (level variation) footprints for a complete revolution. It can be seen that both footprints do not change significantly beyond a distance of a few rotor diameters. For both cross-wind directions, the *average* level is lower than in the up- and downwind directions, but the *variation* in level is larger. Even at a large distance, trailing edge noise directivity and convective amplification may cause swish amplitudes up to 5 dB in the cross-wind directions. This may be an explanation for the increased amplitude modulation reported in [33–35, 39], although it should be noted that at large distances (beyond several rotor diameters) variations in atmospheric conditions, which are not modeled here, may also cause fluctuations in the perceived noise level. Note that at small distance to the turbine (one rotor diameter) substantial swish is observed in *all* directions, which is consistent with the measurements.

6. CONCLUSIONS

A semi-empirical prediction method for trailing edge noise has been applied to calculate the noise from two modern large wind turbines. The prediction code only needs the blade geometry and the turbine operating conditions as input. Using detailed acoustic array and directivity measurements, a thorough validation of the predictions has been carried out. The predicted noise source distribution in the rotor plane (as a function of frequency and observer position) shows the same characteristics as in the experiments: due to trailing edge noise directivity and convective amplification, practically all noise (emitted to the ground) is produced during the downward movement of the blades, causing a swishing noise during the passage of the blades. Good agreement is also found between the measured and predicted spectra, in terms of levels and spectral shape. For both turbines, the deviation between predicted and measured overall sound levels (as a function of rotor power) is less than 1-2 dB, which is smaller than the scatter in the experimental data. Using a smoothed analytical trailing edge noise directivity function, the turbine noise directivity is predicted within 1-2 dB, and the swish amplitude in different directions within 1 dB. This semi-empirical directivity function shows similar characteristics as the theoretical directivity function for a flat plate, except for regions close to the plane of the blade. The validated prediction code is then applied to calculate noise footprints of the wind turbine as a function of rotor azimuth. These footprints show that for cross-wind directions the *average* level is lower than in the up- and downwind directions, but the *variation* in level is larger. Even at large distance, swish amplitudes up to 5 dB can be expected for cross-wind directions.

ACKNOWLEDGMENTS

REFERENCES

[1] F. van den Berg, E. Pedersen, J. Bouma, R. Bakker, WINDFARM perception: Visual and acoustic impact of wind turbine farms on residents - Final report, 2008.

[2] S. Wagner, R. Bareiss, G. Guidati, *Wind Turbine Noise*. Springer Verlag, 1996.

[3] G. Guidati, J. Ostertag, S. Wagner, Prediction and reduction of wind turbine noise: an overview of research activities in Europe, American Institute of Aeronautics and Astronautics Paper 2000–0042, 2000.

[4] J.E. Ffowcs Williams, L.H. Hall, Aerodynamic sound generation by turbulent flow in the vicinity of a scattering half plane, *Journal of Fluid Mechanics* 40 (1970), 657–670.

[5] R.K. Amiet, Noise due to turbulent flow past a trailing edge. *Journal of Sound and Vibration* 47 (1976) 387–393.

[6] M.S. Howe, A review of the theory of trailing edge noise. *Journal of Sound and Vibration* 61 (1978) 437–465.

[7] R.H. Schlinker, R.K. Amiet, *Helicopter rotor trailing edge noise*, NASA CR-3470, 1981.

[8] W.K. Blake, *Mechanics of Flow-Induced Sound and Vibration*, Academic Press, 1986.

[9] T.F. Brooks, D.S. Pope, M.A. Marcolini, *Airfoil Self-Noise and Prediction*. NASA Reference Publication 1218, 1989.

[10] T. Dassen, R. Parchen, G. Guidati, S. Wagner, S. Kang, A.E. Khodak, Comparison of measured and predicted airfoil self-noise with application to wind turbine noise reduction, *Proceedings of the European Wind Energy Conference*, Dublin, October 1997.

[11] G. Guidati, R. Bareiss, S. Wagner, T. Dassen, R. Parchen, Simulation and measurement of inflow-turbulence noise on airfoils, American Institute of Aeronautics and Astronautics Paper 97–1698, 1997.

[12] M.S. Howe, Edge-source acoustic Green's function for an airfoil of arbitrary chord with application to trailing-edge noise, *The Quarterly Journal of Mechanics and Applied Mathematics* 54, 2001.

[13] A.A. Oberai, F. Roknaldin, T.J.R. Hughes, Computation of Trailing-Edge Noise Due to Turbulent Flow over an Airfoil, *AIAA Journal*, Vol. 40, No. 11, 2002.

[14] F.V. Hutcheson, T.F. Brooks, Effects of angle of attack and velocity on trailing edge noise, American Institute of Aeronautics and Astronautics Paper 2004–1031, 2004.

[15] S. Oerlemans, P. Migliore, Aeroacoustic wind tunnel tests of wind turbine airfoils, American Institute of Aeronautics and Astronautics Paper 2004–3042, 2004.

[16] S. Moreau, M. Roger, Competing broadband noise mechanisms in low speed axial fans, American Institute of Aeronautics and Astronautics Paper 2004–3039, 2004.

[17] M. Herr, W. Dobrzynski, Experimental investigations in low noise trailing edge design, American Institute of Aeronautics and Astronautics Paper 2004–2804, 2004.

[18] M. Roger, S. Moreau, Back-scattering correction and further extensions of Amiet's trailing-edge noise model. Part 1: theory, *Journal of Sound and Vibration* 286 (2005) 477–506.

[19] P.J. Moriarty, G. Guidati, P. Migliore, Prediction of turbulent inflow and trailing-edge noise for wind turbines, American Institute of Aeronautics and Astronautics Paper 2005–2881, 2005.

[20] T. Lutz, A. Herrig, W. WÅrz, M. Kamruzzaman, E. Krämer, Design and wind tunnel verification of low noise airfoils for wind turbines, *American Institute of Aeronautics and Astronautics Journal*, Vol 45, No. 4, 2007, pp 779–792.

[21] S. Glegg, B. Morin, O. Atassi, R. Reba, Using RANS Calculations of Turbulent Kinetic Energy to Provide Predictions of Trailing Edge Noise, American Institute of Aeronautics and Astronautics Paper 2008–2993, 2008.

[22] R.D. Sandberg, N.D. Sandham, Direct numerical simulation of turbulent flow past a trailing edge and the associated noise generation, *Journal of Fluid Mechanics* 596 (2008), 353–385.

[23] A. de Bruijn, W.J. Stam, W.B. de Wolf, Determination of the acoustic source power levels of wind turbines, *Proceedings of the European Wind Energy Conference*, Hamburg, October 1984.

[24] F.W. Grosveld, Prediction of broadband noise from large horizontal axis wind turbine generators, American Institute of Aeronautics and Astronautics Paper 84-2357, 1984.

[25] S.A.L. Glegg, S.M. Baxter, A.G. Glendinning, The prediction of broadband noise from wind turbines, *Journal of Sound and Vibration* 118 (1987) 217–239.

[26] H.H. Hubbard, K.P. Shepherd, Aeroacoustics of large wind turbines, *Journal of the Acoustical Society of America* 89 (1991) 2495–2508.

[27] M.V. Lowson, Theory and experiment for wind turbine noise, American Institute of Aeronautics and Astronautics Paper 94–0119, 1994.

[28] P. Fuglsang, H.A. Madsen, *Implementation and verification of an aeroacoustic noise prediction model for wind turbines*, Risø-R-867(EN), Risø National Laboratory, 1996.

[29] M.V. Lowson, J.V. Lowson, A.J. Bullmore, Wind turbine noise: analysis of results from a new measurement technique, American Institute of Aeronautics and Astronautics Paper 98–0037, 1998.

[30] P. Moriarty, P. Migliore, *Semi-empirical aeroacoustic noise prediction code for wind turbines*. NREL/TP-500-34478, National Renewable Energy Laboratory, Golden, CO, 2003.

[31] W.J. Zhu, N. Heilskov, W.Z. Shen, J.N. Sørensen, Modeling of aerodynamically generated noise from wind turbines, Journal of Solar Energy Engineering (2005), Vol. 127, 517–528.

[32] G. Leloudas, W.J. Zhu, J.N. Sørensen, W.Z. Shen, S. Hjort, Prediction and reduction of noise from a 2.3 MW wind turbine, *Proceedings of The Science of Making Torque from Wind*, Journal of Physics: Conference Series 75 (2007).

[33] P. Dunbabin, An investigation of blade swish from wind turbines, Proceedings of Internoise 96, 463–469, 1996.

[34] G.P. van den Berg, Effects of the wind profile at night on wind turbine sound, *Journal of Sound and Vibration* 277, 2004.

[35] A. Moorhouse, M. Hayes, S. von Hünerbein, B. Piper, M. Adams, Research into aerodynamic modulation of wind turbine noise: final report, University of Salford, July 2007.

[36] S. Oerlemans, P. Sijtsma, B. Méndez López, Location and quantification of noise sources on a wind turbine, *Journal of Sound and Vibration* 299, 2007.

[37] S. Oerlemans, J.G. Schepers, Prediction of wind turbine noise and comparison to experiment, *Proceedings of the Second International Meeting on Wind Turbine Noise*, Lyon, France, September 2007.

[38] S. Oerlemans, M. Fisher, T. Maeder, K. Kögler, Reduction of wind turbine noise using optimized airfoils and trailing-edge serrations, American Institute of Aeronautics and Astronautics Paper 2008–2819, 2008.

[39] D. Bowdler, Amplitude modulation of wind turbine noise, Acoustics Bulletin of the Institute of Acoustics (UK), Vol. 33, No. 4, July/August 2008.

[40] IEC norm 61400-11, Wind turbine generator systems - Acoustic noise measurement techniques, 2002.

[41] D.H. Johnson, D.E. Dudgeon, *Array Signal Processing*, Prentice Hall, 1993.

[42] S. Oerlemans, L. Broersma, P. Sijtsma, Quantification of airframe noise using microphone arrays in open and closed wind tunnels, *International Journal of Aeroacoustics*, Vol. 6, Nr. 4, 2007.

[43] P. Sijtsma, S. Oerlemans, H. Holthusen, Location of rotating sources by phased array measurements, American Institute of Aeronautics and Astronautics Paper 2001–2167, 2001.

[44] P. Sijtsma, R.W. Stoker, Determination of Absolute Contributions of Aircraft Noise Components using Fly-Over Array Measurements, American Institute of Aeronautics and Astronautics Paper 2004–2958, 2004.

[45] B.H. Bulder, S.A.M. Barhorst, J.G. Schepers, F. Hagg, Theory and user's manual BLADOPT, ECN-C-01-011, , Energy Research Centre of the Netherlands ECN, 2001.

[46] B. Montgomerie, A. Brand, J. Bosschers, R. van Rooij, Three-dimensional effects in stall, ECN-C-96-079, Energy Research Center of the Netherlands ECN, 1997.

[47] M. Drela, XFOIL: An analysis and design system for low Reynolds number airfoils, Low Reynolds number aerodynamics, T. J. Mueller, Ed., University of Notre Dame, Paris, 1989.

[48] E.T.G. Bot, Aerodynamische Tabel Generator (in Dutch), ECN-C-01-077, Energy Research Centre of the Netherlands ECN, 2001.

[49] M.R. Fink, Noise component method for airframe noise, *AIAA Journal of Aircraft*, Vol. 17, No. 10, 1979.

[50] T.F. Brooks, C.L. Burley, Rotor broadband noise prediction with comparison to model data, American Institute of Aeronautics and Astronautics Paper 2001–2210, 2001.

[51] A.P. Dowling and J.E. Ffowcs Williams, *Sound and sources of sound*, Ellis Horwood Limited, 1983.